24th COBEM - 2017

24th ABCM International Congress of Mechanical Engineering
December 3-8, 2017, Curitiba, PR, Brazil

COBEM-2017-1217
INFLUENCE OF OPERATIONAL CONDITIONS ON THE AIR BUBBLE DYNAMICS INSIDE A CENTRIFUGAL PUMP

Edgar M. Ofuchi
Felipe C. Ancajima
Renzo G. H. Sabino
Henrique Stel
Dalton Bertoldi
Moises A. Marcelino Neto
Rigoberto E. M. Morales
Multiphase Flow Research Center (NUEM), Federal University of Technology – Paraná (UTFPR) Rua Deputado Heitor Alencar Furtado, 5000 - Curitiba, Brasil
edgarofuchi@gmail.com
felancajima@gmail.com
renzo_cs5@hotmail.com
stel.henrique@gmail.com
daltonbertoldi@utfpr.edu.br
mneto@utfpr.edu.br
rmorales@utfpr.edu.br

Abstract. *Centrifugal pumps operate below their desired capacity when subject to gas-liquid flows. Several studies were developed to understand the effect of gas on the pump performance, but just a few are interested in understanding the gas phase dynamics inside the pump. In this sense, this work presents an experimental and numerical study on the influence of operational conditions on the bubble dynamics in a centrifugal pump. High-speed photography is used to track the motion of isolated bubbles inside the pump impeller. Numerically, the flow of bubbles inside the pump first stage is simulated using an Euler-Lagrange "one way" approach. Comparison between numerical and experimental results shows a good agreement. Results reveal that the operating conditions have an important influence on the bubble trajectory. Higher flow rates help to drag the bubbles outside the impeller, while increasing the rotational speed can force the bubbles back to the pump inlet. The motion of bubbles is also very sensitive to their. Study of the bubble dynamics as influenced by different operating conditions is key to understand the mechanisms behind the performance degradation of pumps with gas-liquid flows.*

Keywords: *Pump, gas-liquid, bubble motion, experimental, numerical.*

1. INTRODUCTION

Understanding the operation of centrifugal pumps with gas-liquid flows is a matter of great interest of some industrial areas. Relevance of the topic include loss-of-coolant accidents (LOCA) in nuclear reactors and petroleum production in oil wells where Electric Submersible Pumps (ESPs) are used. It is known that the performance of pumps is degraded when handling gas-liquid mixtures. This is mainly caused due to gas accumulation in the impeller channels, which affects the liquid flow passage and impairs the ability of the pump to increase pressure.

Studies about this subject concentrate on performance evaluation of centrifugal pumps working with gas-liquid flows under different operating conditions, such as Lea and Bearden (1982), Sachdeva et al. (1994), Pessoa and Prado (2003), Caridad et al. (2008), Trevisan and Prado (2011) and Gamboa and Prado (2012). However, fewer studies, as Murakami and Minemura (1974), bring a comprehensive analysis of the gas dynamics inside impellers in order to understand the effect of the flow pattern in performance degradation.

Numerical studies on two-phase flow in pumps are scarce. The existing works often employ Euler-Euler approaches to investigate the gas distribution inside the impellers, for example Barrios (2007) and Zhu et al. (2017). In turn, Minemura and Murakami (1980) used a Lagrangian "one way" approach to investigate bubble trajectories in a radial impeller. However, the authors only validated their model with one operating condition in a restricted area of the impeller.

Due to the lack of studies on the subject, this work presents an analysis of the motion of bubbles inside a centrifugal pump. High-speed photography is used to evaluate the trajectories of isolated bubbles inside the impeller, while a "one-way" Euler-Lagrange method is used to solve the bubble trajectories in equivalent conditions. Analysis of the effect of operating conditions on the gas dynamics in impellers helps to understand the mechanism of performance degradation in gas-liquid pumping.

2. EXPERIMENTAL AND NUMERICAL METHODS

Figure 1-(a) shows the experimental setup used in this investigation. Liquid and gas lines are mixed to generate a liquid flow with dispersed bubbles through a commercial pump, whose original casing and impeller are replaced by equivalent transparent pieces. A booster pump is used to push the liquid to the pump test. Using a high-speed camera, isolated bubbles are photographed as they flow through the impeller, while its rotating speed and liquid flow rate are controlled. Reference dimensions are used to perform a pixel-position correlation in order to evaluate the bubble trajectories (Fig. 1-(b)).

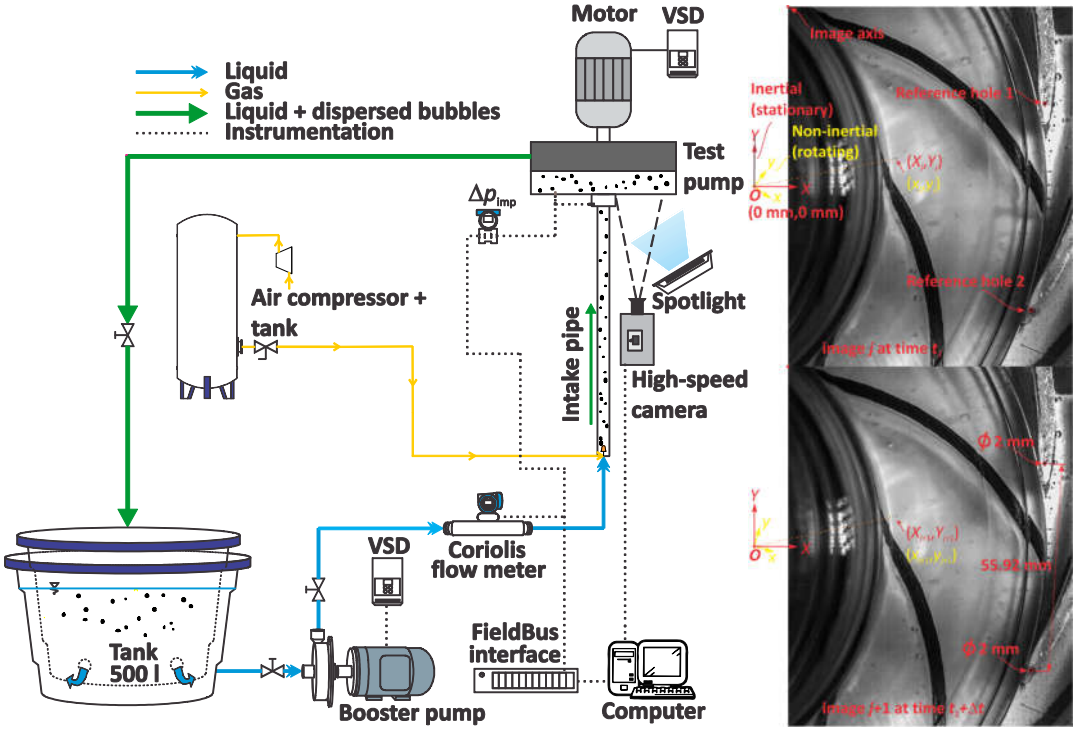

Figure 1: (a) Experimental loop for visualization of bubbles inside a pump impeller, (b) sequence of images showing the bubble position and reference dimensions.

The single-phase, turbulent, isothermal and incompressible flow inside the centrifugal pump is governed by the continuity and momentum equations, represented in Eqs. (1) and (2).

$$\nabla . \boldsymbol{V}_{xyz} = 0 \tag{1}$$

$$\rho \frac{D\boldsymbol{V}_{xyz}}{Dt} = -\nabla p + \mu_{eff} \nabla^2 . \boldsymbol{V}_{xyz} + \rho_l \boldsymbol{g} - 2\rho_l (\boldsymbol{\Omega} \times \boldsymbol{V}_{xyz}) - \rho_l \boldsymbol{\Omega} \times (\boldsymbol{\Omega} \times \boldsymbol{r}) , \tag{2}$$

$\boldsymbol{V}_{xyz}$ is the velocity vector in the rotating frame of reference, $\boldsymbol{\Omega}$ is the angular velocity vector, $\boldsymbol{r}$ is the position vector of a liquid particle with respect to the coordinate frame origin, ρ_l is the liquid density, p is the pressure, $\boldsymbol{g}$ is the gravity acceleration and t is time. The effective viscosity, μ_{eff}, is the sum of the liquid dynamic viscosity, μ_l, and the eddy viscosity, μ_t, a term that comes from the Boussinesq hypothesis and is modeled using the k-ω SST turbulence model. The rotating frame gives rises to the Coriolis and Centrifugal forces represented by the last two terms on the

right-hand side of Eq. (2). When the flow passes the impeller and enters the diffuser, the Coriolis and Centrifugal forces vanish from Eq. (2), and a static frame of reference is adopted.

The Lagrangian solution, used to model the motion of individual bubbles through the liquid, assumes the bubble as a point particle. Then, Newton's second law is applied to integrate the bubble trajectory from a given initial position up to an arbitrary final integration time, or until the particle leaves the solution domain.

After the solution of the continuous liquid phase, the bubbles motion are calculated separately. The bubbles are assumed as small and spherical without heat or interphase mass transfer.

Applying Newton's second law on a point-particle of mass m_p yields:

$$m_p \frac{d\boldsymbol{V}_p}{dt} = \sum \boldsymbol{F}_{total} \quad , \tag{3}$$

where $\boldsymbol{V}_p$ is the bubble velocity and $\sum \boldsymbol{F}_{total}$ represent the sum of all forces acting on the bubble that result from its interaction with the surrounding liquid. This force can be roughly divided into two forces, interfacial force, $\boldsymbol{F}_{\text{int}}$, and field force, $\boldsymbol{F}_{field}$. The first is composed by forces that act near the bubble, like drag force. While the field force is globally presented independently of the particle motion, like gravity force and pressure gradient force. The relevant forces that compose $\sum \boldsymbol{F}_{total}$, found in literature are:

$$\sum \boldsymbol{F}_{total} = \boldsymbol{F}_{\text{int}} + \boldsymbol{F}_{field} = (\boldsymbol{F}_d + \boldsymbol{F}_{\text{vm}} + \boldsymbol{F}_L + \boldsymbol{F}_{WL} + \boldsymbol{F}_{TD} + \boldsymbol{F}_B) + (\boldsymbol{F}_g + \boldsymbol{F}_r + \boldsymbol{F}_p) \tag{4}$$

where $\boldsymbol{F}_d$, $\boldsymbol{F}_{\text{vm}}$, $\boldsymbol{F}_L$, $\boldsymbol{F}_{WL}$, $\boldsymbol{F}_{TD}$, and $\boldsymbol{F}_B$ are the drag force, virtual mass force, lift force, wall lubrication force, turbulent dispersion force and the Basset force, respectively, which compose the interfacial force. The forces that compose the field force are $\boldsymbol{F}_g$, $\boldsymbol{F}_r$ and $\boldsymbol{F}_p$, which are the gravity force, rotational force (a term that accounts the Coriolis and centrifugal forces), and the liquid pressure gradient force that acts on the bubble, respectively.

However, not all forces are relevant to the two-phase flow in centrifugal pumps. Following the study of Minemura and Murakami (1980), the forces that most affect the bubble trajectory are the drag force, the virtual mass force, the rotating force and the pressure gradient force. This hypothesis is used here and the other forces will be neglected. Thus, Eq. (3) is now given by:

$$m_p \frac{d\boldsymbol{V}_p}{dt} = \boldsymbol{F}_d + \boldsymbol{F}_{\text{vm}} + \boldsymbol{F}_p + \boldsymbol{F}_r \, . \tag{5}$$

The drag force acting from the liquid on the bubble is calculated for a spherical bubble of diameter D as:

$$\boldsymbol{F}_d = -\frac{1}{2} C_d \rho_l (\boldsymbol{V}_b - \boldsymbol{V}_l) \left| \boldsymbol{V}_b - \boldsymbol{V}_l \right| \frac{\pi D^2}{4} , \tag{6}$$

where $(\boldsymbol{V}_b - \boldsymbol{V}_l)$ is the relative velocity between the bubble velocity, $\boldsymbol{V}_b$, and the liquid velocity, $\boldsymbol{V}_l$. ρ_l is the liquid density and C_d is the drag coefficient, which is dependent on the particle Reynolds number:

$$Re = \frac{\rho_l \, \mathrm{D}(\boldsymbol{V}_b - \boldsymbol{V}_l)}{\mu_l} , \tag{7}$$

where μ_l is the liquid dynamic viscosity. Within $0 < Re < 1000$, a well known expression for C_d in terms of Re for spherical particles is given by the Schiller-Naumann correlation (Ansys, 2015):

$$C_d = \frac{24}{Re}(1 + 0{,}15 Re^{0{,}687}) \, . \tag{8}$$

For higher Reynolds numbers, the drag coefficient is assumed constant, $C_d = 0.44$.

The virtual mass force is proportional to the displacement of a portion of liquid mass by the movement of the bubble. The acceleration of the liquid and gas phases is accounted both temporally and spatially. In this work, steady

state liquid films are taken as the continuum for which the particle moves. Thus, only the advective part of the liquid filed and the Coriolis effect are considered in the virtual mass force, which is given by (Ansys, 2015):

$$\boldsymbol{F}_{vm} = \frac{C_{vm}}{2} m_l \left[-\boldsymbol{V}_l \nabla \boldsymbol{V}_l + 2\boldsymbol{\Omega} \times (\boldsymbol{V}_b - \boldsymbol{V}_l) \right] , \tag{9}$$

where $m_l = \rho_l \pi D^3 / 6$ is the mass of the displace liquid and C_{vm} is the virtual mass coefficient. For an isolated spherical particle, a value of 0.5 is normally taken for C_{vm} .

The pressure gradient force, $\boldsymbol{F}_p$, is obtained from the liquid pressure gradient. It is proportional to the pressure gradient of the liquid phase, ∇p , and the bubble volume, $\pi D^3 / 6$, and acts on the bubble according to the following expression:

$$\boldsymbol{F}_P = -\frac{\pi D^3}{6} \nabla p , \tag{10}$$

Finally, rotational force, $\boldsymbol{F}_r$, is given by the sum of Coriolis and centrifugal forces:

$$\boldsymbol{F}_r = m_b \left[-2\boldsymbol{\Omega} \times \boldsymbol{V}_b - \boldsymbol{\Omega} \times \boldsymbol{\Omega} \times \boldsymbol{r}_b \right] \tag{11}$$

where $2\boldsymbol{\Omega} \times \boldsymbol{V}_b$ and $\boldsymbol{\Omega} \times \boldsymbol{\Omega} \times \boldsymbol{r}_b$ are the Coriolis and the centrifugal accelerations.

The governing equations presented earlier are solved through commercial CFD software ANSYS® CFX® Release 15.0 (Ansys, 2015). This software uses a multi-block technique to solve the flow in centrifugal pumps, in which, each part of the pump is a sub-domain with its own frame of reference. The sub-domains are connected through interface models that account for the tangential displacement of rotating parts and disarranged meshes between each side of the interface. Steady state simulations were performed in which the "Frozen Rotor" was adopted. This model considers the rotational source (Coriolis and Centrifugal forces) in the momentum equation, while the relative position between the impeller and a static component is kept fixed.

Element based Finite Volume method is employed to solve Eqs. (1) and (2) for the liquid phase. A High Resolution advection scheme is used to interpolate the advection terms (Ansys, 2015). A co-located grid is used to couple the pressure-velocity through the Rhie and Chow (1983) approach. The k-ω SST turbulence model is adopted to model turbulence (Menter, 1994).

Hexahedral body-fitted elements were used to build the domain mesh with the aid of ANSYS® ICEM CFD™ and ANSYS® TurboGrid™ softwares. Figure 2-(a) shows the numerical grid mesh of the centrifugal pump used in this work. Mesh refinement was made near all walls, specially near the blade walls. A mesh sensitivity test was conducted and it was verified that a mesh with around 1,200,000 nodes is adequate for the purposes of this work, in which, the impeller alone accounts for more than 1,000,000 nodes.

After the solution of the liquid phase, bubbles are released in the domain and its motion is calculated through Eq. (5). The numerical solution is straightforward, using for example the regular first order Euler integration method (Ansys, 2015). The initial positions of the bubbles were gathered from the experimental work of Sabino (2015) for sake of comparison and validation.

The governing equations are solved in the pump domain, shown schematically in Fig. 2-(b), which is based on a radial type Imbil ITAP 65-330/2 centrifugal pump with two impellers. However, in this study the domain was limited to one stage (one impeller and one diffuser). Thus the geometry is composed by one suction pipe, one impeller, one diffuser and a simplified extension of the diffuser. The latter was used to put the outlet far from the diffuser outlet, which brings numerical stability to the problem. The impeller has 8 blades and the diffuser has 12 vanes. Figure 2-(b) also shows the boundary conditions applied in this problem. At the inlet, a fixed reference pressure of 0 [Pa] is set. A specified flow rate is imposed at the diffuser extension outlet. All walls are smooth and non-slip.

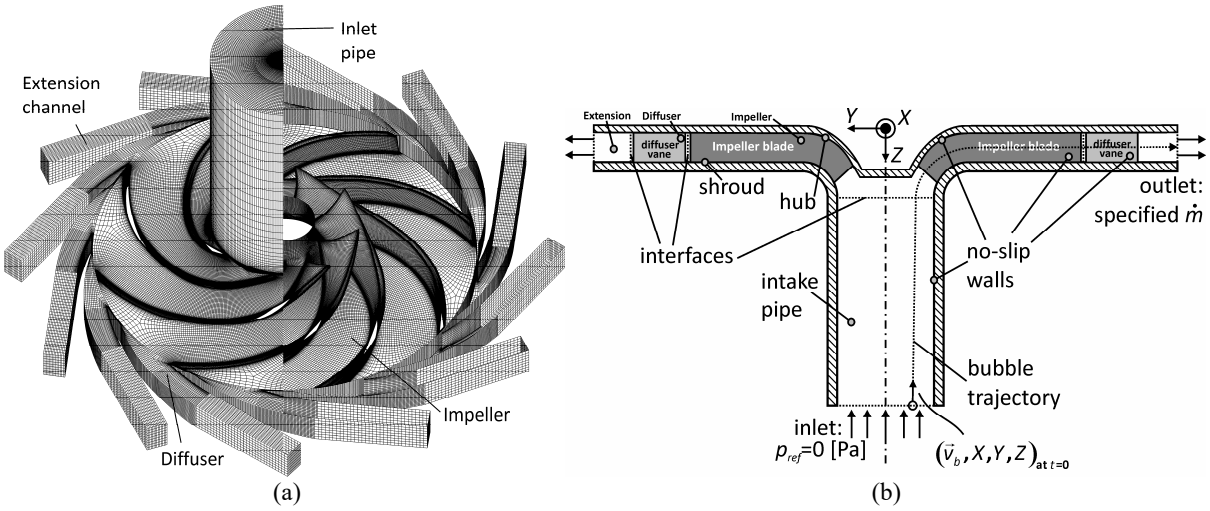

Figure 2: Numerical domain: (a) mesh; (b) boundary conditions.

3. RESULTS AND DISCUSSION

The bubble trajectory is presented in one channel of the centrifugal pump, in which the channel is limited by the blades B1 and B2. In addition, curves of blade hub and leading edge are shown to elucidate the reader about the position and the trajectory of the bubble inside the impeller.

Numerical and experimental bubble trajectory are compared and shown in Fig. 3. Figure 3-(a) shows the trajectory of bubbles with different diameters at 100 rpm and at the Best Efficiency Point (BEP) flow rate. Numerical and experimental results have a quite similar bubble trajectory. In addition, it is observed that bubbles go to the pressure side of B1 and then to the impeller inlet. However, the bigger bubble went to the pressure side earlier than the smaller bubble. This is due to the pressure gradient force (Eq. 10), in which it is proportional to the diameter of the bubble to cubic Figure 3-(b) presents bubbles path in the impeller for two bubbles diameters at 220 rpm rotational speed and 1.2×BEP flow rate. A good agreement between numerical and experimental results is observed, even the bubble deflection to the pressure side is captured by the numerical model. In addition, in this case the bubbles leave the impeller domain.

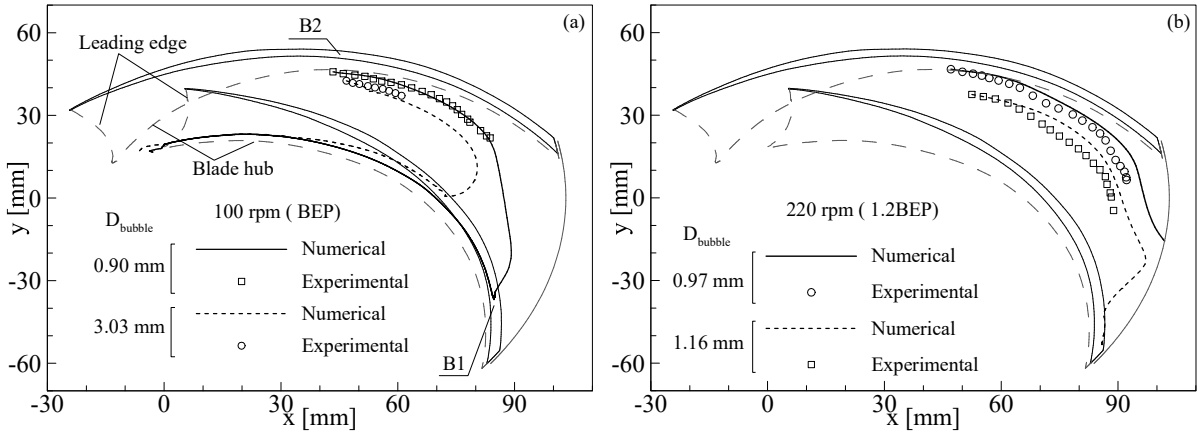

Figure 3: Comparison of experimental and numerical bubble trajectories inside the impeller.

Several forces are considered to influence on the bubble trajectory inside the centrifugal pump. Figure 4 shows the influence of the interfacial forces on the bubble. First, it was considered the influence of the radial and centrifugal forces. Including drag and the pressure gradient forces push the bubble toward the suction side of the blade, while the virtual mass force impacts only near the exit of the impeller.

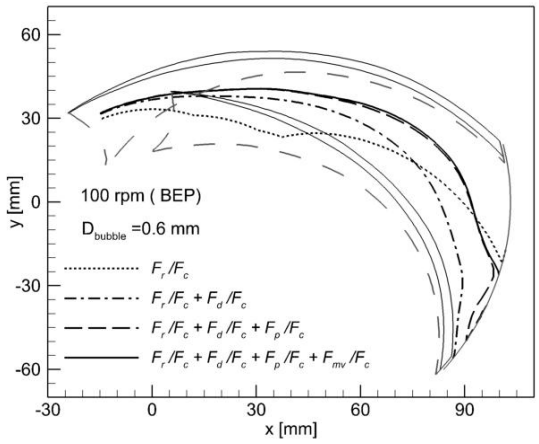

Figure 4. Influence of interfacial force on the bubble trajectory.

Figure 5 presents a single bubble trajectory from the inlet to outlet of the impeller. In Fig. 5-(a), one notice that the drag and pressure gradient forces have the same order of magnitude but opposite directions, whilst the virtual mass force has a small and a non-defined direction vector. The pressure gradient force pushes the bubble toward the impeller inlet, while the drag force pushes to the impeller exit. The balance between these two forces is the key analysis of the present study. It will define if the bubble stay or leave the impeller. Figure 5-(b) shows the magnitude of the drag, pressure gradient and virtual mass forces, in which all forces are normalized by the centrifugal force. The pressure gradient and the drag forces have the same order and is almost in equilibrium. The slightly difference makes the bubble leave the impeller.

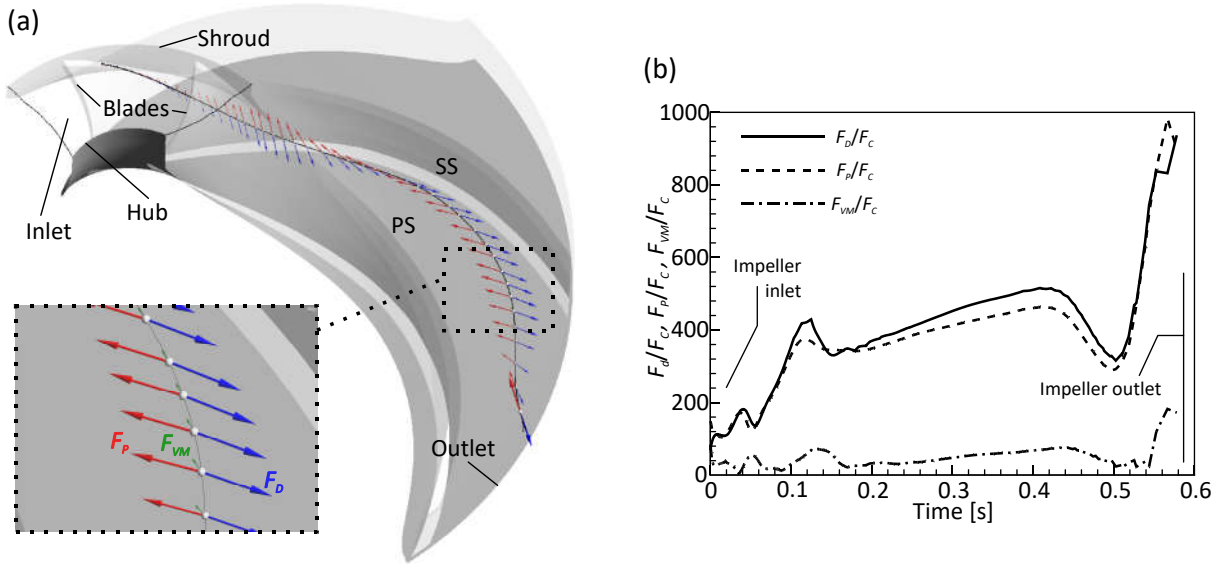

Figure 5. (a) force balance on the bubble and (b) drag, pressure gradient and virtual mass force module as function of time.

Figure 6 presents the influence of the flow rate on the bubble. Increase the flow rate in a centrifugal pump has two effects: first it increase the drag force and second it decrease the pressure gradient force due to the characteristics of the head curve of a back sweep blade impeller. In Fig. 6-(a), one verify that the bubble trajectory is almost the same until the bubble is pushed toward the pressure side of the blade. For 1.0×BEP to 1.2×BEP flow rate, the bubble remains inside the impeller, but goes farther away from the impeller inlet. For 1.3×BEP the bubble leaves the impeller domain. Figure 6-(b) shows the ratio of drag and pressure gradient force as function of the bubble trajectory. For both cases, until the position P_{xy}, the ratio of the forces oscillates due to a contact of the bubble to the blade wall. After the P_{xy} position, the higher flow rate has a greater ratio between the forces respect to the lower flow rate, which aids the bubble to leave the impeller.

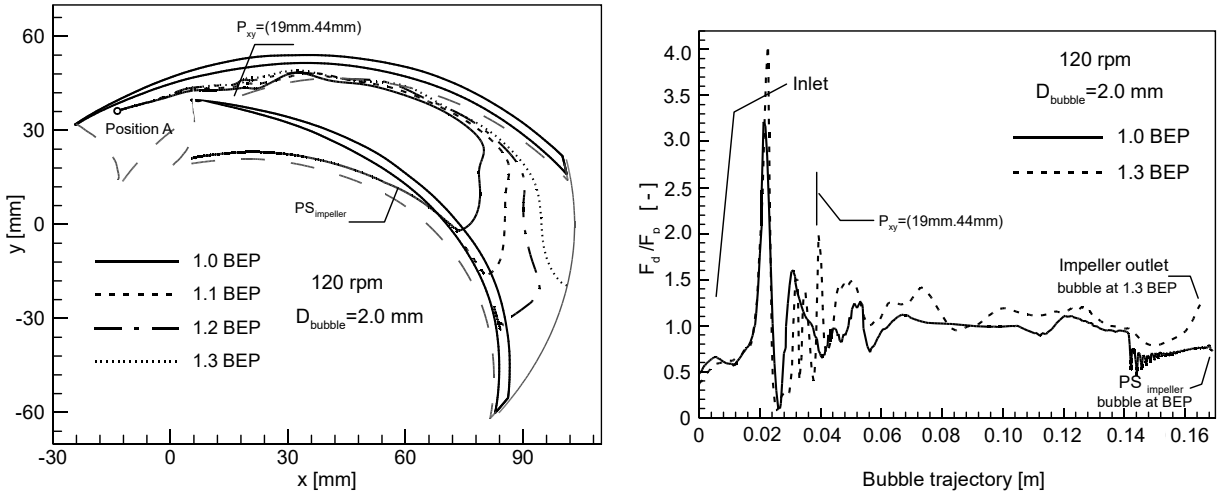

Figure 6. (a) bubble path for different liquid flow rate at 120 rpm and 2.0 mm bubble diameter. (b) Ratio between drag and pressure gradient force as function of the bubble trajectory at 120 rpm, two liquid flow rate and 2.0 mm bubble diameter.

Figure 7-(a) shows the bubble trajectory inside the impeller for different rotation speeds. As the rotation speed rise, the bubble is deflected, near the exit of the impeller, to the pressure side direction. For 220 rpm rotation speed, the bubble goes to the pressure side and stays in the impeller. An increase in rotational speed rise both flow rate and pressure rise, as determined by the similarity laws for centrifugal pumps. However, the increase in pressure rise is square, while for the flow rate is linear. Figure 7-(b) presents the ratio between pressure gradient and drag forces as function of the trajectory of the bubble. One observe that the ratio of the forces behave equally, however, the peaks are higher for 220 rpm and the bubble stay in the impeller, while for 100 rpm the bubble leave the domain.

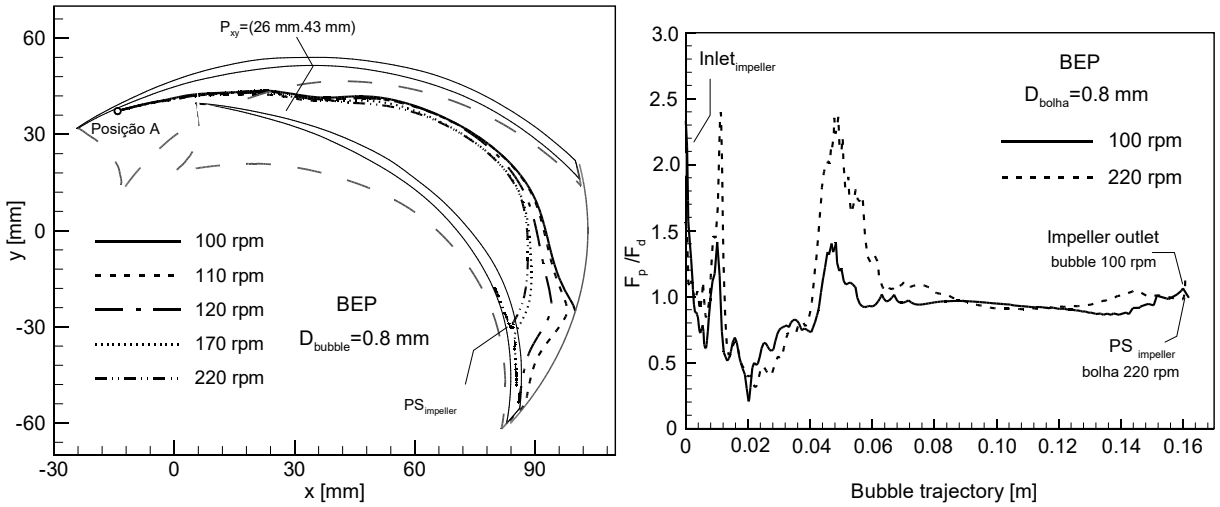

Figure 7. (a) bubble path for different rotational speed for BEP liquid flow rate and 0.8 mm bubble diameter. (b) Ratio between pressure gradient and drag force as function of the bubble trajectory for BEP liquid flow rate, two rotational speeds and 0.8 mm bubble diameter.

4. CONCLUSIONS

Experimental and numerical approaches are used to study the trajectory of bubbles in a pump impeller. Results reveal that the bubble motion is significantly affected by the impeller speed, the bubble diameter and the liquid flow rate. Some conclusions and contributions can be taken of the understand of the two phase flow in centrifugal pumps.

i) Bigger bubble diameter increase the pressure gradient force and increase the chances of the bubble to stay in the impeller

ii) The balance between drag and pressure gradient forces are the main reason for the bubble to stay or leave the impeller.
iii) Higher flow rates increase the drag force on the bubble and push then to the impeller outlet.
iv) Increase in rotational speed rise both pressure gradient and drag forces, which may lead the bubble to stay. In addition, higher rotational speeds push the bubble toward the pressure side of the blade.

5. ACKNOWLEDGES

The authors acknowledge the financial support from CNPq, ANP and FINEP through the Human Resources Program to oil and gas segment PRH-ANP (PRH 10 - UTFPR) and from TE/CENPES/PETROBRAS.

6. REFERENCES

ANSYS, 2015. ANSYS® Academic Research, Release 15.0, Help System, CFX Documentation, ANSYS, Inc.

Barrios, L.J., 2007. *Visualization and Modeling of Multiphase Performance Inside an Electrical Submersible Pump*. PhD dissertation, The University of Tulsa, Tulsa, OK.

Caridad, J., Asuaje, M., Kenyery F., Tremante, A. and Aguillón O., 2008. “Characterization of a centrifugal pump impeller under two-phase flow conditions.” *Journal of Petroleum Science and Engineering,* Vol 63, p 18-22.

Gamboa, J. and Prado, M., 2012. “Experimental Study of Two-Phase Performance of an Electric-Submersible-Pump Stage.” *SPE Production & Operations*, Vol 27 (4), p 414-421.

Lea, J.F. and Bearden J.L., 1982. “Effect of Gaseous Fluids on Submersible Pump Performance.” *Journal Of Petroleum Technology*. Vol 34 (12), p 2922-2930.

Menter, F.R., 1994. “Two-Equation Eddy-Viscosity Turbulence Models for Engineering Applications”, AIAA Journal, Vol. 32, pp. 1598-1605.

Minemura, K. and Murakami M., 1980. "A Theoretical Study on Air Bubble Motion in a Centrifugal Pump Impeller." *Journal of Fluids Engineering* Vol 102 (4), p 446-453.

Murakami, M. and Minemura K., 1974. "Effects of Entrained Air on the Performance of a Centrifugal Pump : 1st Report, Performance and Flow Conditions." *Bulletin of JSME,* Vol 17(110), p 1047-1055.

Pessoa, R. and Prado, M., 2003. "Two-Phase Flow Performance for Electrical Submersible Pump Stages." *SPE Production & Facilities*, Vol 18 (01), p 13-27.

Rhie, C.M. and Chow, W.L., 1983. “Numerical Study of the Turbulent Flow Past an Airfoil with Trailing Edge Separation.” *AIAA Journal*, Vol. 21, pp. 1525-1532.

Sachdeva, R., Doty, D.R. and Schmidt Z., 1994. “Performance of Electric Submersible Pumps in Gassy Wells.” *SPE Production & Facilities*. Vol 9 (1), p 55-60.

Trevisan, F. and Prado, M., 2008. “Experimental Investigation of the Viscous Effect on Two-Phase-Flow Patterns and Hydraulic Performance of Electrical Submersible Pumps.” *Journal of Canadian Petroleum Technology*, Vol 50 (4), p 45-52.

Zhu J, and Zhang, H.Q., 2017. “Numerical Study on Electrical Submersible-Pump Two-Phase Performance and Bubble-Size Modeling.” *SPE Production & Operations*, Vol 32 (3), p 1-12.

7. RESPONSIBILITY NOTICE

The author(s) is (are) the only responsible for the printed material included in this paper.